

First Glance Diagnosis: Brain Disease Classification with Single fMRI Volume

Wei Dai, Ziyao Zhang, Lixia Tian, Shengyuan Yu, Shuhui Wang, Zhao Dong, and Hairong Zheng, *Senior Member, IEEE*

Abstract—In neuroimaging analysis, functional magnetic resonance imaging (fMRI) can well assess brain function changes for brain diseases with no obvious structural lesions. So far, most deep-learning-based fMRI studies take functional connectivity as the basic feature in disease classification. However, functional connectivity is often calculated based on time series of predefined regions of interest and neglects detailed information contained in each voxel, which may accordingly deteriorate the performance of diagnostic models. Another methodological drawback is the limited sample size for the training of deep models. In this study, we propose BrainFormer, a general hybrid Transformer architecture for brain disease classification with single fMRI volume to fully exploit the voxel-wise details with sufficient data dimensions and sizes. BrainFormer is constructed by modeling the local cues within each voxel with 3D convolutions and capturing the global relations among distant regions with two global attention blocks. The local and global cues are aggregated in BrainFormer by a single-stream model. To handle multisite data, we propose a normalization layer to normalize the data into identical distribution. Finally, a Gradient-based Localization-map Visualization method is utilized for locating the possible disease-related biomarker. We evaluate BrainFormer on five independently acquired datasets including ABIDE, ADNI, MPILMBB, ADHD-200 and ECHO, with diseases of autism, Alzheimer’s disease, depression, attention deficit hyperactivity disorder, and headache disorders. The results demonstrate the effectiveness and generalizability of BrainFormer for multiple brain diseases diagnosis. BrainFormer may promote neuroimaging-based precision diagnosis in clinical practice and motivate future study in fMRI analysis. Code is available at: <https://github.com/ZiyaoZhang/orPCL/BrainFormer>.

Index Terms—Functional MRI, brain disease classifica-

Wei Dai and Ziyao Zhang contributed equally.

Corresponding authors: Shuhui Wang; Zhao Dong.

Wei Dai, Shengyuan Yu, and Zhao Dong are with the Department of Neurology, Chinese PLA General Hospital, Beijing 100853, China (e-mail: daiwei@plagh.org, yusy1963@126.com, dong.zhaozhao@126.com).

Ziyao Zhang and Hairong Zheng are with the Paul C. Lauterbur Research Center for Biomedical Imaging, Shenzhen Institutes of Advanced Technology, Chinese Academy of Sciences, Shenzhen, Guangdong 518000, China and Peng Cheng Laboratory, Shenzhen, Guangdong 518000, China (e-mail: zhangzy@pcl.ac.cn, hr.zheng@siat.ac.cn).

Lixia Tian is with the School of Computer and Information Technology, Beijing Jiaotong University, Beijing 100044, China (e-mail: lxtian@bjtu.edu.cn).

Shuhui Wang is with the Institute of Computing Technology, Chinese Academy of Sciences, Beijing 100190, China (e-mail: wangshuhui@ict.ac.cn).

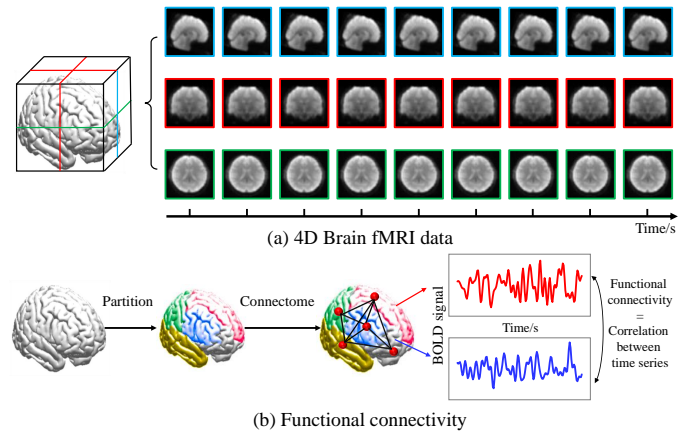


Fig. 1. (a) 4D brain fMRI data: 3D volumes of the brain along temporal dimension, and sections of sagittal, coronal and axial views are shown for better visualization; (b) the functional connectivity between two brain areas is calculated by the Pearson correlation coefficients between the time series of the predefined brain region.

tion, Transformer, 3D CNN, global attention.

I. INTRODUCTION

RECENT years have witnessed the great development in artificial intelligence. Thanks to the explosive growth of data and advance of deep learning technology, extensive progresses have been made in areas such as vision [1] and language [2]. Deep learning have been proliferating in medical domains, including digital health, patient monitoring and disease diagnostics. Among them, imaging based diagnosis has drawn researchers’ attention because of its precious value in application. With the rapid growth of medical imaging data [3], methods designed for structural segmentation, lesion detection and disease classification also developed [4], [5].

Magnetic resonance imaging (MRI) is a powerful non-invasive tool for disease diagnosis. The structural MRI (sMRI) records the detailed structure in the internal body, which can well reflect the signals of lesion areas for consequent diagnosis and treatment. The sMRI analysis is particularly useful on complex organs such as the brain, and promising progresses have been achieved recently [6]. However, sMRI appears to be less effective on those brain diseases that present no obvious structural changes, e.g., psychological disorders, autism, and headache disorders. These diseases are traditionally treated as brain functional disorders and diagnosed based on clinical

interviews and behavioral assessments. And the diagnostic accuracy of these diseases depends largely on doctor's professionalism. Thus, to explore neuroimaging-based diagnosis could improve precision in medical practice.

In comparison with sMRI, functional MRI (fMRI) is an effective technique to reflect the functional organization of the brain. fMRI uses blood oxygen level dependent (BOLD) signal as a measure of neural activity along temporal dimension. However, as an indirect measure of neural activity, effective models are needed to analyze the actual brain functional fluctuations underlying fMRI data.

The fMRI data item can be regarded as a 4D tensor, which consists of a sequence of scanned 3D brain volumes arranged along the temporal dimension¹, with each voxel in the 3D volume recording the BOLD signal of a specific brain region in a given time interval. Due to the computational limitation, early researchers designed functional connectivity (FC) feature instead of directly using the fMRI data tensor. The FC records the pair-wise Pearson correlation coefficients between a set of predefined brain regions of interest (ROI), where two ROIs are assumed to be functionally connected if they display synchronous functional activity fluctuations, as shown in Fig. 1. By squeezing the original 4D tensor into low dimensional vector, the FC among different brain ROIs of much lower dimensions (relative to the original 4D tensor) can be obtained. The FC patterns have been playing an essential role in traditional classification models, on which any off-the-shelf classifiers, *e.g.*, Support Vector Machine (SVM) [7] or specially designed deep learning methods, *e.g.*, multi-channel Deep Neural Network [8]–[10], can be employed for brain disease detection.

However, FC-based diagnostic models have often been reported to be of relatively low accuracies. The FC feature is built on the whole 4D tensors with predefined brain regions, which merely encodes the overall correlation between pairwise brain regions by using all the 3D volumes. The strategy of calculating FC based on mean time series across voxels within brain regions leads to the extremely low dimension of FC and accordingly insufficient information for later classifications. Due to the coarse granularity of FC feature, the disease-related biomarker may be hard to detect even with strong deep neural networks. Worse still, due to the physical difference among MRI scanners used in different study sites, the FC features calculated on one fMRI dataset can hardly be calibrated and aligned to the data of others, and this leads to the poor generalizability of the features across datasets and different brain diseases.

To overcome the insufficient feature representation ability in fMRI analytics, we consider deep feature learning directly on the fMRI data volume. On each 3D volume, we apply 3D Convolution Neural Network (CNN) [11]–[14] to capture the detailed and informative features inside the 3D signal. To alleviate the distribution divergence among data volumes collected from multiple sites, we design a data normalization layer to align the data distributions of different fMRI sources. Compared to previous FC-based brain disease classification

frameworks, our feature extraction framework can be trained in an end-to-end fashion directly on the 3D volume inputs without any manual brain region labeling. It enhances the available training data size by hundreds of times through using volume-wise feature instead of the subject-wise FC feature. It avoids the drastic information losses brought by FC feature, thus the feature representation ability appears to be stronger. Moreover, by normalizing the data, our feature learning mechanism is more generalizable across data sources and brain diseases.

Furthermore, the key in detecting the brain diseases lies in the mechanism of modeling the FC among different brain areas in a more fine-grained manner, instead of the long-term statistics. Traditional deep neural networks, *e.g.*, CNN and Residual Neural Networks, are believed to model the feature correlation within a comparatively short spatial-temporal range. Recently, Transformer is introduced to capture the long-range relationships among features, by computing a fully connected attention mask to learn relation between different visual patches. It has been proved to be particularly effective and achieves state-of-the-art accuracy in various vision tasks including object detection [15], semantic segmentation [16] and video action recognition [17]. In our study, by collaborating with 3D CNN that captures the local feature correlations, the global attention of Transformer offers us the ability to learn the correlation between distant brain regions. Nevertheless, the major technical challenge in applying Transformer to fMRI analysis lies in the prohibitive computation complexity on the high-dimensional fMRI data, especially at shallow layers with high feature resolution.

In this paper, we propose BrainFormer, an universal brain disease classification model based on single fMRI volume working in an ROI-labeling free manner. We design two attention blocks to reach better computational efficiency. A Shallow Global Attention (SGA) block is designed for shallow layers to efficiently exchange information globally through fully connected layer, while the Deep Global Attention (DGA) block is designed for deep layers to accurately fuse global information through global attention mask. The two types of global attention blocks are combined in a unified framework for 3D fMRI volume classification. Based on BrainFormer, we further propose a Gradient-based Localization-map Visualization (GLV) approach to locate possible brain biomarkers to identify the disease. GLV computes class-dependent saliency map based on the gradients back-propagated from specific class, which further increases the discriminability of the learned feature. We evaluate our method on five independently acquired brain disease datasets, including ABIDE, ADNI, MPILMBB, ADHD-200 and ECHO. The diseases include major depressive disorder (MDD), Alzheimer's disease (AD) and mild cognitive impairment (MCI), autism spectrum disorder (ASD) and Asperger's syndrome (AS), attention deficit hyperactivity disorder (ADHD), migraine disease (MD) and medication-overuse headache (MOH). Our method achieves state-of-the-art performance on all the five brain diseases.

The contribution of this work is summarized as follows:

- We propose BrainFormer, a Transformer-based brain disease classification model that can generalize to data from

¹Typically, there are hundreds of volumes in a 4D tensor.

multiple study sites. To our best knowledge, this is the first attempt on classification from single fMRI volume using Transformer. It demonstrates strong generalizability on five types of brain diseases.

- BrainFormer can well capture both local and distant feature correlation at different levels by specifically designed SGA and DGA. Meanwhile it restores the original information within fMRI volume through Gradient-based Localization-map Visualization, for which we can precisely locate the disease-related biomarkers. BrainFormer facilitates diagnosis of brain diseases in clinical practice.
- Experiments on five independent datasets with eight types of brain diseases validate the generalizability and transferability of our approach on brain disease diagnosis.

II. RELATED WORK

Brain fMRI classification: fMRI is a powerful tool to explore brain's functional alterations and fluctuations. Extensive studies on fMRI-based classification mainly focused on FC, which characterizes the pairwise correlation between two predefined brain regions [18]–[20]. Wang *et al.* [18] performed sparse multiview task-centralized ensemble learning for ASD binary classification with age and sex information combined with FC features. Wang *et al.* [19] proposed functional correlation tensor combined with FC that could take advantage of both grey and white matter features, and performed multi-source domain adaptation and multi-view sparse representation to achieve 3-class ASD classification. A Recent study by Wang *et al.* [20] directly conducted 3-class classification on ASD by introducing label distribution learning to FC feature matrix and the labels described shared or specific disease features of the subjects. There are a few studies taking single fMRI volume for disease classification [21], [22]. Vu *et al.* [21] built a vanilla 3D CNN for single fMRI volume classification, which consisted of 3 convolution layer hence lost the correlation cues between distant regions.

3D CNN: 3D CNN is a common method to process 3D signal like video or 3D point cloud. 3D CNN encodes the spatial-temporal cues or 3D structure through sliding 3D convolution kernel along consecutive video frames [13], [23]. Tran *et al.* [11] designed a convolution 3D network (C3D) through directly stacking several 3D convolution layers. However, the 3D CNN lacks pretrained parameters on large-scale datasets, which increases the model training difficulty. Carreira *et al.* [23] built a deep Inflated 3D (I3D) network through inflating the 2D convolution kernels in 2D CNN to the corresponding 3D kernels. Qiu *et al.* [13] factorized the 3D convolution kernels into 2D spatial kernel and 1D temporal kernel, which significantly reduced the parameters without performance drop. Li *et al.* [12] built a compact Multi-scale 3D (M3D) convolution to learn multi-scale temporal cues with dilated temporal convolution. 3D CNN has demonstrated promising performance in 3D signal processing, which is suitable for fMRI data. However, 3D CNN only encodes local cues, hence it's unable to capture long range relation among distant brain regions in MRI analysis. 3D CNN is designed for data from single site, which suffers serious performance drop when directly applied to multisites fMRI data.

Transformer: Transformer [2] is first proposed in natural language processing (NLP) to model long range dependencies among tokens. Inspired by the successes in NLP, recent work tried to introduce Transformer into computer vision tasks [15], [17], [24]. Wang *et al.* [17] proposed a Non-Local (NL) neural network for action recognition to learn long-range dependencies inside and cross video frames. Carion *et al.* [15] designed a DETection TRansformer (DETR) for object detection. DETR does not require any specialized operation like anchor definition or non-maximum suppression, and demonstrates promising accuracy and efficiency. Dosovitskiy *et al.* [25] proposed a Vision Transformer (ViT) which directly transfers the Transformer to image classification. ViT splits an image into several patches and each patch is treated the same way as word tokens in NLP task. Transformer's strong ability in long range dependencies modeling makes it suitable to capture relations between distant brain regions in fMRI volume. Nevertheless, computing fully connected attention mask for high-dimensional fMRI data may suffer unaffordable computation cost.

In this paper, we propose BrainFormer, an end-to-end architecture for brain fMRI classification based on single volume. Compared with existing methods which rely on FC, our method jointly captures local details inside brain region and global relationship between brain regions from single fMRI volumes, and exhibits stronger capability in brain disease classification. As shown in our experiments, our method achieves competitive performance on various brain disease datasets. Moreover, our method directly make prediction based on fMRI data, hence is more suitable to locate disease-related bio-marker, which may further facilitates the neuroimaging-based brain disease diagnosis in clinical practice.

III. PROPOSED METHOD

A. Formulation

The brain disease classification task aims to classify brain fMRI data into diseased and normal classes. A brain fMRI data of single person can be viewed as a sequence of 3D tensor $\mathbf{V} = \{\mathcal{V}_1, \mathcal{V}_2, \dots, \mathcal{V}_T\}$, $\mathcal{V}_i \in \mathcal{R}^{D \times H \times W}$, where T denotes temporal length, and D , H and W represent depth, height and width of 3D volume at each time point. The fMRI classification can be performed by,

$$p_i = f(\mathcal{V}_i), \quad (1)$$

where $p_i \in \mathcal{R}^n$ denotes the classification score for i -th volume, and n is the predefined class number, *e.g.*, 2 classes for diseased and healthy individual. We use f to denote our classification model BrainFormer. The BrainFormer directly takes 3D fMRI volume as input and outputs the predicted classification score. Fig. 2 illustrates the overall framework of BrainFormer. It consists of a data normalization layer, 3D CNN backbone and global attention blocks. The following parts proceed to introduce each component of BrainFormer.

B. BrainFormer

1) **Data Normalization Layer:** Usually, the fMRI datasets are collected from multiple sites, and the data distribution in one

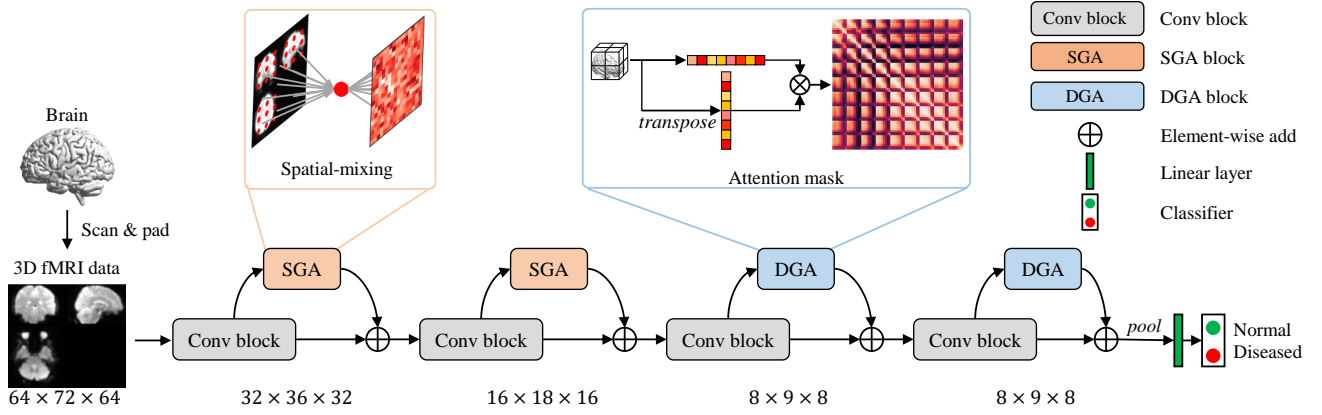


Fig. 2. Overview of the proposed BrainFormer for brain disease classification. BrainFormer consists of a data normalization layer for data normalization, a 3D CNN backbone for feature extraction and two attention blocks SGA and DGA for global correlation learning. SGA: Shallow Global Attention, DGA: Deep Global Attention.

site is different from each other. Therefore, we apply data normalization layer to normalize all fMRI volumes to identical distribution. We apply instance normalization on 3D volume \mathcal{V}_i to normalize it to zero-mean and unit-variance distribution,

$$\bar{\mathcal{V}}_i = \frac{\mathcal{V}_i - \text{mean}(\mathcal{V}_i)}{\text{std}(\mathcal{V}_i)}, \quad (2)$$

where $\bar{\mathcal{V}}_i$ is the normalized volume.

2) **3D CNN Backbone:** We employ 3D CNN as backbone feature extractor. The 3D CNN accepts 3D fMRI volume $\mathcal{V} \in \mathcal{R}^{D \times H \times W}$ as input and outputs the corresponding 3D feature map $\mathbf{f} \in \mathcal{R}^{d \times h \times w}$ (we omit channel dimension for simplicity). Our 3D CNN consists of several convolution blocks, which are made up of 3D convolution layers, batch normalization layers and nonlinear activation layer. The stride of last convolution layer in each block is set as 2.

3D convolution layer: The 3D convolution layer encodes the 3D structural cues through sliding 3D kernel along each dimension of 3D fMRI volume. A 3D convolution kernel can be formulated as a 3D tensor $\mathbf{W} \in \mathcal{R}^{d \times h \times w}$, where d , h and w are the depth, height and width of kernel (the input and output channel are omitted). The computation of a $3 \times 3 \times 3$ sized 3D convolution can be formulated as,

$$\mathbf{f}_{d,h,w}^{\text{out}} = \sum_{i=0}^2 \sum_{j=0}^2 \sum_{k=0}^2 \mathbf{f}_{d-1+i, h-1+j, w-1+k}^{\text{in}} \times \mathcal{W}_{i,j,k}, \quad (3)$$

where \mathcal{W} is the weight of 3D convolution kernel, and \mathbf{f}^{in} and \mathbf{f}^{out} are input and output feature, respectively.

Batch normalization layer: Batch Normalization (BN) layer is inserted to mitigate this internal covariate shift [26] and speed up training. A BN layer is achieved through a normalization step and a transformation step,

$$\hat{x} = \gamma \frac{x - \mu}{\sqrt{\sigma^2 + \epsilon}} + \beta, \quad (4)$$

where μ and σ are mean and variance for normalization, and γ and β are learnable parameters for scaling and shifting,

Nonlinear activation layer: We employ ReLU layer to provide nonlinear ability in BrainFormer,

$$\phi(x) = \max(0, x) = \begin{cases} x, & \text{if } x \geq 0, \\ 0, & \text{if } x < 0. \end{cases} \quad (5)$$

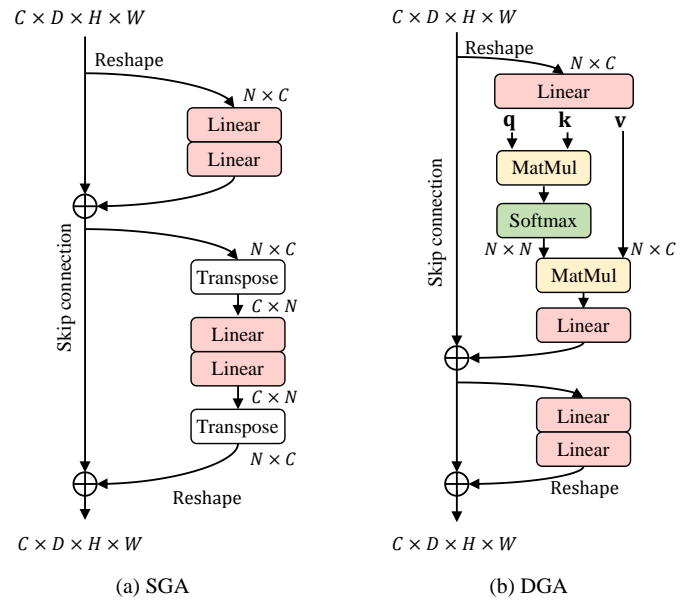


Fig. 3. The detailed structure of (a) Shallow Global Attention block which consists of spatial-mixing block and channel-mixing block, and (b) Deep Global Attention block which consists of Multi-head Self-Attention and Feed-Forward layer. $N = D \times H \times W$ is the total number of feature.

The positive values are kept and negative values are set to 0.

3) **Global Attention Block:** 3D CNN only encodes information inside each local region, but it's unable to capture the correlation between distant brain regions. The self-attention is widely used to formulate global relationship in computer vision and natural language processing tasks [2], [15], [24]. Traditional self-attention learns global relationship through computing fully connected attention mask for 1D/2D input signal. However, the attention computation for 3D fMRI volume will suffer unaffordable computation complexity, especially on the high resolution feature in shallow layer. Towards more effective attention modeling for fMRI data, we design different attention blocks for shallow and deep layer, respectively.

Shallow Global Attention block: Fig. 3(a) depicts the detailed structure of Shallow Global Attention (SGA). It accepts a sequence of volume features, shaped as “#seq×channels” as

input, and uses two Multi-Layer Perceptron (MLP) blocks for spatial-mixing and channel-mixing, respectively. The spatial-mixing block allows communication between different spatial locations, by operating on each channel independently. The channel-mixing block allows information communication between different channels. These two types of blocks are interleaved to enable interaction among input dimensions.

The input 3D feature is first flattened to $x \in \mathcal{R}^{N \times C}$, where C is the number of channels, and $N = D \times H \times W$ is the resulting number of features, which also serves as the input sequence length. The first MLP block acts on columns of x to mix global spatial information, and the second MLP block acts on the rows of x to mix the channel information. Each MLP block contains two fully-connected layers with nonlinear mapping,

$$\begin{aligned} x'_{*,i} &= x_{*,i} + \mathbf{W}_2^S \phi(\mathbf{W}_1^S x_{*,i}), \quad \text{for } i = 1 \dots C, \\ x''_{j,*} &= x'_{j,*} + \mathbf{W}_4^S \phi(\mathbf{W}_3^S x'_{j,*}), \quad \text{for } j = 1 \dots N, \end{aligned} \quad (6)$$

where ϕ is ReLU activation layer, and \mathbf{W}_1^S , \mathbf{W}_2^S , \mathbf{W}_3^S and \mathbf{W}_4^S are weights of fully connected layers. Both MLP blocks are inserted with residual connection. \mathbf{W}_4^S is initialized as zero to keep original initialization. For input $x \in \mathcal{R}^{N \times C}$, SGA reduces the computational complexity of self-attention from $\mathcal{O}(N^2)$ to $\mathcal{O}(N)$, relieving the memory and computation costs in shallow layers where the feature resolution is high.

Deep Global Attention block: Deep Global Attention (DGA) is designed to fuse the global information in deep layer. Fig. 3(b) depicts the detailed structure of DGA. Considering that the computation complexity of MSA is $\mathcal{O}(N^2)$, we only insert it into deep layers. A DGA block consists of a Multi-head Self-Attention (MSA) and a Feed Forward (FF) layer. Similarly, DGA also flattens the input to $x \in \mathcal{R}^{N \times C}$. Extra position embedding $\mathbf{E}_{pos} \in \mathcal{R}^{N \times C}$ is added to volume features to retain the positional information. The resulting feature sequence serves as the input to the DGA block. The computation of DGA block can be formulated as,

$$\begin{aligned} z_0 &= x + \mathbf{E}_{pos}, \\ z_1 &= \text{MSA}(z_0) + z_0, \\ z_2 &= \text{FF}(z_1) + z_1. \end{aligned} \quad (7)$$

An MSA layer consists of multiple Self-Attentions (SA). A standard SA can be formulated as mapping a query \mathbf{q} , key \mathbf{k} and value \mathbf{v} to an output, where queries, keys, values, and output are all volume features. The output is computed as a weighted sum of values, where the weight for each value is computed by a similarity function between query and key.

For input features $z \in \mathcal{R}^{N \times C}$, SA first computes \mathbf{q} , \mathbf{k} , and \mathbf{v} through fully connected layer. The attention mask \mathbf{M} is then computed through pairwise similarity between \mathbf{q} and \mathbf{k} ,

$$\begin{aligned} \mathbf{q}, \mathbf{k}, \mathbf{v} &= \mathbf{W}_1^D z, \\ \mathbf{M} &= \text{softmax}(\mathbf{q}\mathbf{k}^T / \sqrt{C_h}), \\ \text{SA}(\mathbf{v}) &= \mathbf{M}\mathbf{v}, \end{aligned} \quad (8)$$

where $\mathbf{W}_1^D \in \mathcal{R}^{C \times 3C_h}$ is the learnable weight matrix in fully connected layer, C_h is the channel number of \mathbf{q}, \mathbf{k} and \mathbf{v} , $\sqrt{C_h}$ is scale factor for normalization, and $\mathbf{M} \in \mathcal{R}^{N \times N}$ is

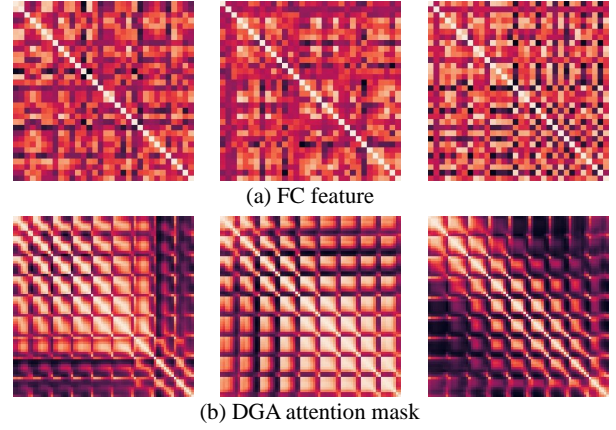


Fig. 4. Visualization of (a) Functional Connectivity (FC) feature, and (b) global attention mask in DGA. Compared with FC, DGA can automatically learn global correlation between finer brain regions.

the attention mask. Softmax function is used to normalize the attention mask to probabilities. MSA is an extension of SA in which k SA are computed in parallel,

$$\text{MSA}(z_0) = [\text{SA}_1(z_0), \dots, \text{SA}_k(z_0)] \mathbf{W}_2^D, \quad (9)$$

where $\mathbf{W}_2^D \in \mathcal{R}^{kC_h \times C}$ is weight matrix of linear layer. The \mathbf{W}_2^D is initialized as zero to keep the original initialization. Finally, the weighted sum of value is added to original input,

$$z_1 = z_0 + \text{MSA}(z_0), \quad (10)$$

where $z_1 \in \mathcal{R}^{N \times C}$ is output of MSA. The MSA layer can effectively capture the global correlation between distant brain regions.

Besides MSA, each DGA block contains an extra FF layer. An FF layer consists of two fully connected layers with ReLU activation, and the output of FF layer is added to input feature with residual manner,

$$\begin{aligned} \text{FF}(z_1) &= \max(0, \mathbf{W}_3^D z_1 + b_1) \mathbf{W}_4^D + b_2, \\ z_2 &= z_1 + \text{FF}(z_1), \end{aligned} \quad (11)$$

where \mathbf{W}_3^D and \mathbf{W}_4^D are weights of fully connected layers in FF, and z_2 is the final output of DGA block.

We visualize the FC feature and a representative attention mask in DGA of 3 randomly selected samples in Fig. 4. FC maps were computed based on Pearson correlations among the mean time series of predefined ROI obtained through statistical algorithms. Differently, the attention map in DGA automatically learns correlation between finer brain voxel through end to end training, hence could learn more reliable correlations.

4) Classifier: The output feature map is pooled with global average pooling and then classified with classifier. A classifier consists of a fully connected layer to map the feature to class index, and a softmax function normalizes the predicted probability to $[0, 1]$,

$$p_i = \frac{e^{\mathbf{W}x_i}}{\sum_{j=1}^n e^{\mathbf{W}x_j}}, \quad (12)$$

where \mathbf{W} is the weight of fully connected layer, n is the class number, and p is the normalized classification score. We

TABLE I

EVALUATION OF INDIVIDUAL COMPONENTS IN PROPOSED METHOD

Name	output size	layers
input	$64 \times 72 \times 64$	-
stem conv	$32 \times 36 \times 32$	$7 \times 7 \times 7$, 64, stride 2
conv block1	$32 \times 36 \times 32$	$\begin{bmatrix} 3 \times 3 \times 3, 64 \\ 3 \times 3 \times 3, 64 \end{bmatrix} \times 2$ SGA block
conv block2	$16 \times 18 \times 16$	$\begin{bmatrix} 3 \times 3 \times 3, 128 \\ 3 \times 3 \times 3, 128 \end{bmatrix} \times 2$ SGA block
conv block3	$8 \times 9 \times 8$	$\begin{bmatrix} 3 \times 3 \times 3, 256 \\ 3 \times 3 \times 3, 256 \end{bmatrix} \times 2$ DGA block
conv block4	$8 \times 9 \times 8$	$\begin{bmatrix} 3 \times 3 \times 3, 512 \\ 3 \times 3 \times 3, 512 \end{bmatrix} \times 2$ DGA block
classifier	$1 \times 1 \times 1$	average pool, 512 \rightarrow c fc, softmax

choose cross-entropy loss to optimize our model,

$$\mathcal{L}_{ce} = - \sum_{i=1}^n l_i \log(p_i), \quad (13)$$

where l_i is one-hot label for classification.

With the designed data normalization layer, 3D CNN and global attention blocks, we build BrainFormer based on 3D ResNet18 [27]. The overall framework is illustrated in Fig. 2, the detailed structure is summarized in Table I.

C. Gradient-based Localization-map Visualization

Since our method directly predicts disease classification on 3D brain fMRI volume, it's more precise to locate disease-related biomarker than FC-based method. In this section, we propose a Gradient-based Localization-map Visualization (GLV) to find disease-related biomarker based on gradient.

To obtain localization map $L^m \in \mathcal{R}^{d \times h \times w}$ for a specific class m at specific intermediate layer, we first compute gradient for class m with respect to activation map $\mathbf{f} \in \mathcal{R}^{c \times d \times h \times w}$ at this layer, e.g., $\frac{\partial y_m}{\partial \mathbf{f}_{ijk}^q}$. We assign importance weight a_m^q to the q -th channel through averaging gradient,

$$a_m^q = \frac{1}{d \times h \times w} \sum_{i=1}^d \sum_{j=1}^h \sum_{k=1}^w \frac{\partial y_m}{\partial \mathbf{f}_{ijk}^q}, \quad (14)$$

where a_m^q is the importance weight of the q -th channel, y_m is the classification score of the m -th class in the classifier.

During the computation of a_m^q , the gradient from the final classification score y_m back propagated to intermediate layer \mathbf{f} . Hence the weight a_m^q captures the importance of the k -th channel for class m . Based on a_m^q , we combine feature map to obtain the localization map with respect to class m ,

$$L^m = \text{ReLU} \left(\sum_{q=1}^c a_m^q \mathbf{f}^q \right). \quad (15)$$

We apply extra ReLU operation to keep the positive activation which has positive influence on class m . To remove class-

irrelevant activation, we subtract average localization map,

$$\hat{L}^m = L^m - \frac{1}{n} \sum_{i=1}^n L^i. \quad (16)$$

Finally, we average the localization maps of all fMRI volumes from the same sequence to obtain the final localization map,

$$\bar{L}^m = \frac{1}{T} \sum_{t=1}^T \hat{L}_t^m. \quad (17)$$

We resize localization map to input size through trilinear interpolation for better visualization.

IV. EXPERIMENT

A. Dataset

We evaluate our method on five independently acquired neuroimaging datasets in Table II.

MPILMBB dataset [28] contains 426 fMRI sequences from 318 individuals, including 228 with MDD and 198 healthy controls (HC). The individual who underwent more than one scan was labeled as either depression or HC. Data used in this study was obtained from the MPI-Leipzig Mind-Brain-Body project².

ADNI we include participants from ADNI2 and ADNI GO datasets [29]. Participants are from 55 study sites from the United States and Canada and include AD, MCI, and HC. We filter the samples with irregular shapes, and finally get 448 fMRI sequences. Most existing methods conducted binary classification (AD vs. HC, or MCI vs. HC) on ADNI dataset. In this paper, we report both binary and 3-class classification performance. ADNI dataset can be accessed from the Alzheimer's Disease Neuroimaging Initiative project³.

ABIDE dataset [30] has aggregated fMRI data of 988 subjects acquired from 17 neuroimaging centers around the world with different imaging protocols. The dataset includes 339 individuals suffering from ASD and 93 suffering from AS, and 546 HC. The majority of studies conducted binary classification (ASD vs. HC) on ABIDE dataset. We report both binary and 3-class classification performance. ABIDE dataset can be accessed from the Autism Brain Imaging Data Exchange project⁴.

ADHD-200 dataset⁵ [31] contains 1,151 subjects with fMRI including 309 ADHD individuals and 842 HC. This dataset was acquired from 8 different neuroimaging centers around the world.

ECHO we have collected a novel fMRI dataset *Evaluation and Classification of Headache disOrders*, (ECHO) from 2 study sites. Two types of headache in ECHO dataset, including MD, MOH, as well as HC are included in the analysis, which consists 107, 38 and 52 individuals, respectively.

²MPILMBB dataset is available on <https://www.neuroconnlab.org/data/>

³ADNI dataset is available on <https://adni.loni.usc.edu>

⁴ABIDE dataset is available on <http://preprocessed-connectome-s-project.org/abide/index.html>

⁵ADHD-200 dataset is available on http://fcon_1000.projects.nitrc.org/indi/adhd200/

TABLE II
THE STATISTICS OF FIVE BRAIN DISEASE DATASETS

Dataset	#individual	#healthy control	#diseased	#class	disease category	volume number
MPILMBB	426	198	228	2	MDD	657
ADNI	448	167	127AD, 154MCI	3	AD, MCI	145
ABIDE	988	556	339ASD, 93AS	3	ASD, AS	82-320 (avg:194)
ADHD-200	1,151	842	309	2	ADHD	76-261 (avg:162)
ECHO	187	52	107MD, 38MOH	3	MD, MOH	240

MDD: major depressive disorder, AD: Alzheimer’s disease, MCI: mild cognitive impairment, ASD: autism spectrum disorder
AS: Asperger’s syndrome, ADHD: attention deficit hyperactivity disorder, MD: migraine disease, MOH: medication-overuse headache

B. Implementation Details

1) *Data Preprocessing*: Before training, we preprocess all fMRI data except ABIDE and ADHD-200 using DPARSF toolset⁶ based on MATLAB2013b (8.2.0.701). The pipeline includes the following steps: (1) remove the first 5 volumes; (2) slice timing correction; (3) realignment to correct for motion; (4) normalize fMRI data to Montreal Neurological Institute (MNI) standard space through DARTEL and resample to $3 \times 3 \times 3$ mm³ resolution; (5) spatial smoothing with a 6-mm (full width at half maximum, FWHM) Gaussian kernel. Above process results $T \times 61 \times 73 \times 61$ tensor for each fMRI sequence, where T is the length of sequence. As for ABIDE dataset, the Configurable Pipeline for the Analysis of Connectomes (CPAC) minimally preprocessed data [30] is used. The pipeline is as follows: (1) slice timing correction; (2) realignment to correct for motion; (3) write into template space at $3 \times 3 \times 3$ mm³ isotropic resolution. For ADHD-200 dataset, the Athena preprocessed data [31] is used and the pipeline is based on tools from the AFNI and FSL software packages: (1) remove the first 4 volumes; (2) slice timing correction; (3) deoblique dataset; (4) reorient into RPI orientation; (5) motion correct volumes to the first (originally 5th) image of the time series; (6) mask the dataset to exclude non-brain; (7) average the volumes to create a mean image; (8) co-register mean fMRI image to corresponding anatomic image; (9) write fMRI data and mean image into template space at $4 \times 4 \times 4$ mm³ isotropic resolution; (10) down-sample white matter and cerebrospinal fluid (CSF) masks to match fMRI resolution; (11) extract WM and CSF time-courses from fMRI volumes using WM and CSF masks; (12) regress out WM, CSF, motion time courses as well as a low order polynomial from fMRI data; (13) blur the data using a 6-mm FWHM Gaussian filter.

2) *Training*: For BrainFormer training, we apply 3D ResNet18 [23] as backbone feature extractor and initialize it with weights pretrained on ImageNet [1]. All our models are trained with Adam optimizer for 10 epochs, and each batch contains 16 3D volumes. The initial learning rate is set as 0.0001, and is reduced by factor of 10 at 8-th epoch. The 3D volumes are padded to $64 \times 72 \times 64$ before input to model. All models are trained with only cross entropy loss.

3) *Testing*: During testing, we pad input 3D fMRI data to $64 \times 72 \times 64$ for classification. We average the predicted classification scores of all volumes to obtain final prediction of each individual. We use 5-fold cross validation to verify our

TABLE III
CONFUSION MATRIX FOR CLASSIFICATION

Ground Truth	Predicted	
	Positive	Negative
Positive	True Positive (TP)	False Negative (FN)
Negative	False Positive (FP)	True Negative (TN)

TABLE IV
EVALUATION OF THE EFFECTIVENESS OF INDIVIDUAL COMPONENTS IN BRAINFORMER

Method	MPILMBB	ADNI	ABIDE	ADHD	ECHO
BrainFormer	97.2	95.3	72.0	72.5	81.2
w/o data norm	94.2	93.8	58.7	56.7	79.3
w/o SGA	95.3	93.4	68.7	69.2	75.0
w/o DGA	94.7	92.2	67.9	68.5	75.9
w/o SGA, DGA	94.1	90.6	65.5	67.1	73.9

method on MPILMBB, ADNI, ABIDE and ECHO datasets, and report the average performance. For participants who have several scans in one dataset, the splitting ensures fMRI data from the same individual enter either training or testing data. Since ADHD-200 dataset provides split of train and test data, we follow the protocol to verify our method on ADHD-200.

4) *Evaluation Metric*: We report accuracy, precision, recall and F1 score to verify BrainFormer. The confusion matrix for performance computation is explained in Table III.

Accuracy is the ratio of correctly predicted individuals to the total individuals: $Acc. = \frac{TP+TN}{TP+TN+FP+FN}$.

Recall (Sensitivity) is the ratio of correctly predicted positive individuals to all positive individuals: $Recall = \frac{TP}{TP+FN}$.

Precision is the ratio of correctly predicted positive individuals to total predicted positive individuals: $Prec. = \frac{TP}{TP+FP}$.

F1 score is the harmonic average of precision and recall: $\frac{1}{F1} = \frac{1}{2} \left(\frac{1}{Prec.} + \frac{1}{Recall} \right)$.

C. Ablation study

1) *Individual Component*: This section investigates the effectiveness of each component in BrainFormer, including data norm layer, SGA and DGA. The experimental results on five datasets are summarized in Table IV. In the table, “BrainFormer” denotes the complete BrainFormer model, “w/o” refers to discard corresponding component.

It can be observed from table that, without data normalization, BrainFormer suffers large performance drop on all

⁶<http://rfmri.org/DPARSF>

TABLE V
CLASS-WISE PERFORMANCE ON ECHO DATASET

Method	Acc.	Prec.	Recall	F1 score
MD	79.3	74.6	81.5	77.9
MOH	85.8	74.9	61.9	67.8
Healthy control	93.1	88.9	89.0	88.9

TABLE VI
EVALUATION OF FUNCTIONAL CONNECTIVITY

Method	MPILMBB	ADNI	ADHD	ABIDE	ECHO
FC	74.4	73.4	66.7	69.7	58.6
BrainFormer	97.2	95.3	72.0	72.5	81.2
BrainFormer+FC	97.2	95.2	72.2	72.8	81.2

five datasets. This shows our data normalization layer can effectively unify the distribution of multisite data. The largest performance drop can be observed on ABIDE and ADHD-200 dataset, *e.g.*, 13.3% and 15.8%, respectively. The reason may be that ABIDE and ADHD-200 consist of more study sites hence benefit more from data normalization. Table IV also shows that, both SGA and DGA significantly boost the performance. By combining SGA and DGA, BrainFormer achieves the best performance, *e.g.*, Acc=81.2% on ECHO dataset. We hence could conclude that, both SGA and DGA are effective to model the correlation between distant brain areas, it thus enhances the performance of BrainFormer. Their combination achieves the best performance. This shows the global correlation learning in shallow and deep layers is complementary to each other.

2) *Class-wise Analysis on ECHO dataset*: The ECHO dataset contains 3 classes, *e.g.*, MD, MOH, HC, the overall metric cannot measure the performance for each class. Therefore, we evaluate class-wise performance on ECHO dataset in Table V. It can be observed from Table V that, our method achieves superiority recall on MD class. This shows our method can effectively avoid missed diagnosis for MD in clinical practice. Table V also shows that, our method achieves 93.1% accuracy on HC class. This shows our method is able to accurately diagnose healthy individuals based on fMRI data, which may aid doctors in clinical practice.

3) *Comparison with Functional Connectivity*: In this section, we compare BrainFormer with FC based method. Following [9], [32], we extract CC200 to compute FC metric and design a two-layer MLP for FC classification. The comparison results are summarized in Table VI. BrainFormer outperforms FC on all datasets. The reason may be that FC loses the detailed information in each region which is important to distinguish brain disease, while BrainFormer directly works on 3D fMRI data, and preserves important cues. We further combine BrainFormer with FC for joint learning, and get some performance promotion on several datasets. Presumably, the 3D fMRI volumes and FC features contain complementary information for specific brain disease classification.

TABLE VII
COMPARISON WITH REPRESENTATIVE METHODS ON ECHO DATASET

Method	Acc.	Prec.	Recall	F1 score
SVM	33.8	29.0	34.0	31.3
2D CNN	31.2	28.2	31.1	29.6
3D CNN	73.9	72.6	71.6	72.1
3D ViT	68.0	64.7	62.9	65.2
BrainFormer	81.2	79.5	78.4	79.2

TABLE VIII
COMPARISON WITH REPRESENTATIVE METHODS ON MPILMBB DATASET

Method	Acc.	Prec.	Recall	F1 score
MCD [33]	90.0	62.0	75.0	-
BrainFormer	97.2	97.9	97.4	97.7

D. Comparison

In this section, we compare BrainFormer with representative methods on all five datasets.

1) *ECHO*: We first compare BrainFormer on ECHO dataset with machine learning method SVM, and deep learning based methods that include 2D CNN, 3D CNN and 3D ViT [25]. The result is summarized in Table VII. It can be observed from Table VII that, BrainFormer achieves best performance, *e.g.*, 81.2% accuracy, that consistently outperforms all compared methods. Specifically, BrainFormer outperforms ViT by 13.2% on accuracy. Table VII also shows that, 3D CNN achieves 73.9% accuracy, which outperforms 2D CNN by 42.7%. This indicates the importance of 3D information for brain disease classification. Based on 3D CNN, our BrainFormer is equipped extra shallow global attention and deep global attention blocks, which endows 3D CNN global correlation learning ability. This comparison shows the superiority of our method.

2) *MPILMBB*: Table VIII compares BrainFormer with recent works on MPILMBB dataset. It can be observed from Table VIII that, outperforming compared method MCD [33] by large margin.

3) *ADNI*: The comparisons on ADNI dataset is summarized in Table IX. In table IX, our method achieves best performance on ADNI dataset, *e.g.*, 95.3% accuracy for binary classification (AD vs. CN), outperforms the state-of-the-art method Cascaded CNN [34] by 2.1%. Cascaded CNN [34] also uses 3D CNN for fMRI classification. Our method is equipped with two global attention blocks to enhance the global correlation learning ability, hence achieves more reliable classification result. Table IX also shows that, BrainFormer also achieves promising performance for 3-class classification, which further demonstrates the superiority of BrainFormer.

4) *ABIDE*: The comparison results on ABIDE dataset are summarized in Table X. We can see that BrainFormer achieves 72.5% accuracy, outperforming current state-of-the-art ASD-DiagNet [8] on both accuracy and precision. Note that, our method doesn't apply extra data augmentation or auto-encoder for pretraining, hence is more compact and easy to implement. We also provide the performance of 3-class classification in

TABLE IX

COMPARISON WITH REPRESENTATIVE METHODS ON ADNI DATASET

Method	AD vs. HC	MCI vs. HC	3 classes
DeepFusion [35]	76.0	75.0	-
GCN [36]	-	78.0	-
CMTL [37]	90.0	73.0	-
3D ConvNet [38]	90.0	-	-
DenseCNN [39]	90.0	74.0	-
DRN [40]	81.3	-	56.8
Cascaded CNN [34]	93.2	74.3	-
BrainFormer	95.3	89.7	81.2

TABLE X

COMPARISON WITH REPRESENTATIVE METHODS ON ABIDE DATASET

Method	Acc.	Prec.	Recall	F1 score
<i>2 classes</i>				
SVM [10]	64.4	58.6	-	60.4
DRB [41]	66.8	-	-	-
Autoencoder+MLP [10]	67.2	62.3	-	62.6
FCNN [10]	69.8	63.1	-	65.8
GCN [36]	69.5	-	-	-
ASD-DiagNet [8]	70.3	68.3	-	-
BrainFormer	72.5	69.3	65.6	67.4
<i>3 classes</i>				
BrainFormer	67.4	68.0	62.2	65.0

Table X. Our method also achieves comparable performance for 3-class classification.

5) *ADHD-200*: Finally, we compare our method on ADHD-200 dataset, and the results are summarized in Table XI. The compared methods include FCNet [42], 3D CNN [43], DeepFMRI [44], MMTGCN [32], SC-CNN-Attention [45], and MTGCN [32]. From the comparison, we can see that the BrainFormer outperforms DeepFMRI [44], MTGCN [32], and MMTGCN [32] on both accuracy and precision. The results further demonstrate the generalizability and transferability of BrainFormer for multisite fMRI analysis.

E. Visualization

Fig. 5 provides visualization results of disease-related biomarker by GLV on five datasets. The greatest advantage of BrainFormer is that it could directly locate the possible disease-related biomarker on 3D brain volume and provides probability information in the very location. As for traditional

TABLE XI

COMPARISON WITH REPRESENTATIVE METHODS ON ADHD-200 DATASET

Method	Acc.	Prec.	Recall	F1 score
FCNet [42]	64.0	-	-	-
3D CNN [43]	67.8	-	-	-
DeepFMRI [44]	67.9	71.4	-	-
SC-CNN-Attention [45]	68.6	-	-	-
MTGCN [32]	70.6	69.1	-	-
MMTGCN [32]	71.8	71.5	-	-
BrainFormer	72.0	77.7	60.2	67.8

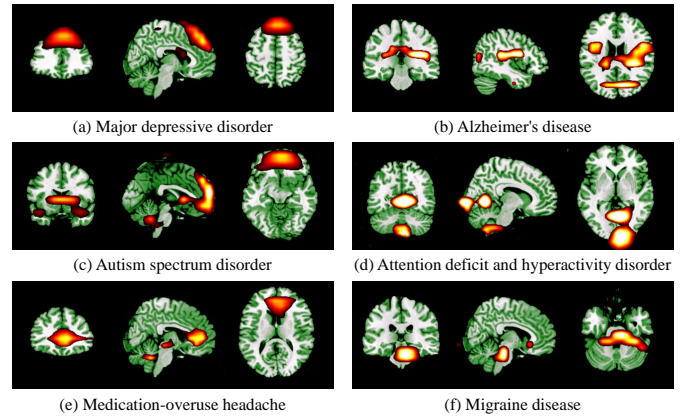


Fig. 5. Visualization results of disease-related biomarker achieved by Gradient-based Localization-map Visualization. The activation map highlights brain regions that are associated with disease classification. (a) from MPILMBB, (b) from ADNI, (c) from ABIDE, (d) from ADHD-200, (e) and (f) from ECHO.

FC, the brain regions are predefined and the mean BOLD value of the predefined regions are computed, making it a blurring method to locate biomarker. Each of the regions illustrated in Fig. 5 has repeatedly been associated with the corresponding disease. As for MDD, the region critical for classification locates mainly in the prefrontal cortex [46]. And the regions may identify AD lie in the frontal, parieto-temporal, and occipital cortex [47]. When it comes to ASD, the prefrontal, temporal, and insular lobe and part of the cerebellum show high response [48]. The related regions for MOH locate in dorsal anterior cingulate cortex [49], the midbrain and cerebellum. As for ADHD, the regions critical for classification locate in the occipital lobe and cerebellum [50]. As for MD, the related regions are brainstem and cerebellum [51].

V. CONCLUSION

This paper proposes BrainFormer, a hybrid Transformer architecture, which uses single volume of fMRI for universal brain disease classification. BrainFormer shows sound generalizability for multiple brain diseases classification, and good transferability for multisite data with different scanning parameters. Visualization results demonstrate the superiority of BrainFormer to directly locate possible disease-related biomarker on fMRI image. The results are achieved by first modeling the local cues within each brain region through 3D CNN, and capturing the global relations among distant regions through two global attention blocks, and then applying a data normalization layer to handle the multisite data. Based on BrainFormer, we further propose a GLV method to locate disease-related biomarker. BrainFormer may promote neuroimaging-based precision diagnosis in clinical practice and motivate future study in fMRI data analysis.

There are still some issues which may influence the performance of BrainFormer. Firstly, we apply a simple normalization layer to handle the multisite data, which could be optimized by better mapping and normalization framework. Secondly, although BrainFormer is capable of classifying multiple diseases, it can only classify one to two diseases of a

spectrum per training. We aim to classify multi-disease in an unified framework through multi-task learning in future work.

REFERENCES

- [1] A. Krizhevsky, I. Sutskever, and G. E. Hinton, "Imagenet classification with deep convolutional neural networks," *Advances in neural information processing systems*, vol. 25, 2012.
- [2] A. Vaswani *et al.*, "Attention is all you need," *Advances in neural information processing systems*, vol. 30, 2017.
- [3] A. Riaz, E. Alonso, and G. Slabaugh, "Phenotypic integrated framework for classification of adhd using fmri," in *International Conference on Image Analysis and Recognition*. Springer, 2016, pp. 217–225.
- [4] D. Wang, Y. Zhang, K. Zhang, and L. Wang, "Focalmix: Semi-supervised learning for 3d medical image detection," in *Proceedings of the Conference on Computer Vision and Pattern Recognition*, 2020, pp. 3951–3960.
- [5] O. Ronneberger, P. Fischer, and T. Brox, "U-net: Convolutional networks for biomedical image segmentation," in *International Conference on Medical image computing and computer-assisted intervention*. Springer, 2015, pp. 234–241.
- [6] C. D. Billones, O. J. L. D. Demetria, D. E. D. Hostallero, and P. C. Naval, "Demnet: a convolutional neural network for the detection of alzheimer's disease and mild cognitive impairment," in *2016 IEEE region 10 conference (TENCON)*. IEEE, 2016, pp. 3724–3727.
- [7] Y. Tang, C. Wang, Y. Chen, N. Sun, A. Jiang, and Z. Wang, "Identifying adhd individuals from resting-state functional connectivity using subspace clustering and binary hypothesis testing," *Journal of attention disorders*, vol. 25, no. 5, pp. 736–748, 2021.
- [8] T. Eslami, V. Mirjalili, A. Fong, A. R. Laird, and F. Saeed, "Asd-diagnet: a hybrid learning approach for detection of autism spectrum disorder using fmri data," *Frontiers in neuroinformatics*, vol. 13, p. 70, 2019.
- [9] M. Chen, H. Li, J. Wang, J. R. Dillman, N. A. Parikh, and L. He, "A multichannel deep neural network model analyzing multiscale functional brain connectome data for attention deficit hyperactivity disorder detection," *Radiology: Artificial Intelligence*, vol. 2, p. e190012, 2019.
- [10] J. Hu, L. Cao, T. Li, B. Liao, S. Dong, and P. Li, "Interpretable learning approaches in resting-state functional connectivity analysis: the case of autism spectrum disorder," *Computational and Mathematical Methods in Medicine*, vol. 2020, 2020.
- [11] D. Tran, L. Bourdev, R. Fergus, L. Torresani, and M. Paluri, "Learning spatiotemporal features with 3d convolutional networks," in *Proceedings of the IEEE international conference on computer vision*, 2015.
- [12] J. Li, S. Zhang, and T. Huang, "Multi-scale 3d convolution network for video based person re-identification," in *Proceedings of the AAAI Conference on Artificial Intelligence*, vol. 33, 2019, pp. 8618–8625.
- [13] Z. Qiu, T. Yao, and T. Mei, "Learning spatio-temporal representation with pseudo-3d residual networks," in *Proceedings of the IEEE international conference on computer vision*, 2017.
- [14] J. Li, S. Zhang, and T. Huang, "Multi-scale temporal cues learning for video person re-identification," *IEEE Transactions on Image Processing*, vol. 29, pp. 4461–4473, 2020.
- [15] N. Carion, F. Massa, G. Synnaeve, N. Usunier, A. Kirillov, and S. Zagoruyko, "End-to-end object detection with transformers," in *European conference on computer vision*. Springer, 2020.
- [16] Z. Huang, X. Wang, L. Huang, C. Huang, Y. Wei, and W. Liu, "Ccnnet: Criss-cross attention for semantic segmentation," in *Proceedings of the International Conference on Computer Vision*, 2019, pp. 603–612.
- [17] X. Wang, R. Girshick, A. Gupta, and K. He, "Non-local neural networks," in *Proceedings of the IEEE conference on computer vision and pattern recognition*, 2018, pp. 7794–7803.
- [18] J. Wang, Q. Wang, H. Zhang, J. Chen, S. Wang, and D. Shen, "Sparse multiview task-centralized ensemble learning for asd diagnosis based on age-and sex-related functional connectivity patterns," *IEEE transactions on cybernetics*, vol. 49, no. 8, pp. 3141–3154, 2018.
- [19] J. Wang *et al.*, "Multi-class asd classification based on functional connectivity and functional correlation tensor via multi-source domain adaptation and multi-view sparse representation," *IEEE transactions on medical imaging*, vol. 39, no. 10, pp. 3137–3147, 2020.
- [20] —, "Multi-class asd classification via label distribution learning with class-shared and class-specific decomposition," *Medical Image Analysis*, vol. 75, p. 102294, 2022.
- [21] H. Vu, H.-C. Kim, M. Jung, and J.-H. Lee, "fmri volume classification using a 3d convolutional neural network robust to shifted and scaled neuronal activations," *NeuroImage*, vol. 223, p. 117328, 2020.
- [22] H. Jang, S. M. Plis, V. D. Calhoun, and J.-H. Lee, "Task-specific feature extraction and classification of fmri volumes using a deep neural network initialized with a deep belief network: Evaluation using sensorimotor tasks," *NeuroImage*, vol. 145, pp. 314–328, 2017.
- [23] J. Carreira and A. Zisserman, "Quo vadis, action recognition? a new model and the kinetics dataset," in *Proceedings of the IEEE conference on computer vision and pattern recognition*, 2017.
- [24] Z. Liu *et al.*, "Swin transformer: Hierarchical vision transformer using shifted windows," in *Proceedings of the International Conference on Computer Vision*, 2021, pp. 10012–10022.
- [25] A. Dosovitskiy *et al.*, "An image is worth 16x16 words: Transformers for image recognition at scale," *arXiv preprint arXiv:2010.11929*, 2020.
- [26] S. Ioffe and C. Szegedy, "Batch normalization: Accelerating deep network training by reducing internal covariate shift," in *International conference on machine learning*. PMLR, 2015, pp. 448–456.
- [27] K. He, X. Zhang, S. Ren, and J. Sun, "Deep residual learning for image recognition," in *Proceedings of the IEEE conference on computer vision and pattern recognition*, 2016, pp. 770–778.
- [28] N. Mendes *et al.*, "A functional connectome phenotyping dataset including cognitive state and personality measures," *Scientific data*, vol. 6, pp. 1–19, 2019.
- [29] R. C. Petersen *et al.*, "Alzheimer's disease neuroimaging initiative (adni): clinical characterization," *Neurology*, vol. 74, no. 3, pp. 201–209, 2010.
- [30] C. Craddock *et al.*, "The neuro bureau preprocessing initiative: open sharing of preprocessed neuroimaging data and derivatives," *Frontiers in Neuroinformatics*, vol. 7, p. 27, 2013.
- [31] P. Bellec, C. Chu, F. Chouinard-Decorte, Y. Benhajali, D. S. Margulies, and R. C. Craddock, "The neuro bureau adhd-200 preprocessed repository," *Neuroimage*, vol. 144, pp. 275–286, 2017.
- [32] D. Yao *et al.*, "A mutual multi-scale triplet graph convolutional network for classification of brain disorders using functional or structural connectivity," *IEEE Transactions on Medical Imaging*, vol. 40, no. 4, pp. 1279–1289, 2021.
- [33] M. Mousavian, J. Chen, Z. Traylor, and S. Greening, "Depression detection from smri and rs-fmri images using machine learning," *Journal of Intelligent Information Systems*, vol. 57, no. 2, pp. 395–418, 2021.
- [34] M. Liu, D. Cheng, K. Wang, and Y. Wang, "Multi-modality cascaded convolutional neural networks for alzheimer's disease diagnosis," *Neuroinformatics*, vol. 16, no. 3, pp. 295–308, 2018.
- [35] U. Senanayake, A. Sowmya, and L. Dawes, "Deep fusion pipeline for mild cognitive impairment diagnosis," in *2018 IEEE 15th international symposium on biomedical imaging*. IEEE, 2018, pp. 1394–1397.
- [36] S. Parisot *et al.*, "Spectral graph convolutions for population-based disease prediction," in *International conference on medical image computing and computer-assisted intervention*. Springer, 2017.
- [37] K. Aderghal, A. Khvostikov, A. Krylov, J. Benois-Pineau, K. Afdel, and G. Catheline, "Classification of alzheimer disease on imaging modalities with deep cnns using cross-modal transfer learning," in *2018 IEEE 31st international symposium on computer-based medical systems (CBMS)*. IEEE, 2018, pp. 345–350.
- [38] K. Bäckström, M. Nazari, I. Y.-H. Gu, and A. S. Jakola, "An efficient 3d deep convolutional network for alzheimer's disease diagnosis using mr images," in *2018 IEEE 15th International Symposium on Biomedical Imaging (ISBI 2018)*. IEEE, 2018, pp. 149–153.
- [39] F. Li *et al.*, "Alzheimer's disease diagnosis based on multiple cluster dense convolutional networks," *Computerized Medical Imaging and Graphics*, vol. 70, pp. 101–110, 2018.
- [40] A. Valliani and A. Soni, "Deep residual nets for improved alzheimer's diagnosis," in *Proceedings of the 8th ACM international conference on bioinformatics, computational biology, and health informatics*, 2017, pp. 615–615.
- [41] A. Abraham *et al.*, "Deriving reproducible biomarkers from multi-site resting-state data: An autism-based example," *NeuroImage*, vol. 147, pp. 736–745, 2017.
- [42] A. Riaz *et al.*, "Fcnnet: a convolutional neural network for calculating functional connectivity from functional mri," in *International Workshop on Connectomics in Neuroimaging*. Springer, 2017, pp. 70–78.
- [43] L. Zou, J. Zheng, C. Miao, M. J. McKeown, and Z. J. Wang, "3d cnn based automatic diagnosis of attention deficit hyperactivity disorder using functional and structural mri," *IEEE Access*, vol. 5, 2017.
- [44] A. Riaz, M. Asad, E. Alonso, and G. Slabaugh, "Deepfmri: End-to-end deep learning for functional connectivity and classification of adhd using fmri," *Journal of neuroscience methods*, vol. 335, p. 108506, 2020.
- [45] T. Zhang *et al.*, "Separated channel attention convolutional neural network (sc-cnn-attention) to identify adhd in multi-site rs-fmri dataset," *Entropy*, vol. 22, p. 893, 2020.
- [46] D. A. Pizzagalli and A. C. Roberts, "Prefrontal cortex and depression," *Neuropsychopharmacology*, vol. 47, no. 1, pp. 225–246, 2022.
- [47] I. M. McDonough, S. B. Festini, and M. M. Wood, "Risk for alzheimer's disease: A review of long-term episodic memory encoding and retrieval fmri studies," *Ageing Research Reviews*, vol. 62, p. 101133, 2020.
- [48] C. M. Murphy *et al.*, "Abnormal functional activation and maturation of ventromedial prefrontal cortex and cerebellum during temporal discounting in autism spectrum disorder," *Human Brain Mapping*, vol. 38, no. 11, pp. 5343–5355, 2017.
- [49] W. Dai *et al.*, "Enhanced functional connectivity between habenula and salience network in medication-overuse headache complicating chronic migraine positions it within the addiction disorders: an ica-based resting-state fmri study," *The Journal of Headache and Pain*, vol. 22, no. 1, pp. 1–9, 2021.
- [50] A. Sathyanesan, J. Zhou, J. Scafidì, D. H. Heck, R. V. Sillitoe, and V. Gallo, "Emerging connections between cerebellar development, behaviour and complex brain disorders," *Nature Reviews Neuroscience*, vol. 20, no. 5, pp. 298–313, 2019.
- [51] W. Dai *et al.*, "Cortical mechanisms in migraine," *Molecular Pain*, vol. 17, p. 17448069211050246, 2021.